Development of a hyperspectral camera for its use in art

Desarrollo de una cámara hiperespectral para su uso en arte

L. Larraya[1*], E. Carretero[1], C. Heras[2]

1. Applied Physics Department, University of Zaragoza, Zaragoza 50009, Spain

2. Electronic and Communications Engineering Department, University of Zaragoza, Zaragoza 50009, Spain

[(*)] E-mail: llarraya@unizar.es   S: miembro de SEDOPTICA / SEDOPTICA member

ABSTRACT:

Hyperspectral imaging was developed by NASA to observe the Earth from space and map the distribution of minerals or vegetation, but its utility has been demonstrated in many different fields. The goal of this work was to build a hyperspectral camera in the visible range of light. To do that, a linear-variable band-pass filter has been used alongside a monochromatic camera and a linear stage with a piezoelectric motor. We obtained a hyperspectral camera capable of measuring in the range of 410 nm to 700 nm and we managed to render color using the reflectance curve. We saw that it is possible to build a camera with enough sensibility to be able to differentiate among similar colors.

Key words: Hyperspectral camera, hyperspectral imaging

RESUMEN:

La fotografía hiperespectral fue desarrollada por la NASA para observar la Tierra desde el espacio y estudiar la distribución de minerales o de vegetación, pero ha demostrado ser útil en muchos otros campos. El objetivo de este trabajo ha sido construir una cámara hiperespectral en el rango visible. Para ello se ha utilizado un filtro variable lineal pasa-banda junto a una cámara monocromática y un motor piezoeléctrico paso a paso. Se ha logrado una cámara hiperespectral capaz de medir en el rango de 410 a 700 nm y conseguimos renderizar el color a partir de la curva de reflectancia. Se observa que es posible construir una cámara con la suficiente sensibilidad para diferenciar entre colores similares.

Palabras clave: Cámara hiperespectral, fotografía hiperespectral

REFERENCES AND LINKS / REFERENCIAS Y ENLACES

[1] C. Cucci, J. K. Delaney, and M. Picollo, "Reflectance hyperspectral imaging for investigation of works of art: old master paintings and illuminated manuscripts",Acc. Chem. Res. **49** (10), (2016).

[2] A. F. Goetz, G. Vane, J. E. Solomon, B. N. Rock, "Imaging spectrometry for Earth remote sensing", Science, **228** (4704), (1985)

[3] Pascucci S, Pignatti S, Casa R, Darvishzadeh R, Huang W. Special Issue "Hyperspectral Remote Sensing of Agriculture and Vegetation". Remote Sens., **12**(21), (2020)

[4] Ma, L., Lu, G., Wang, D. et al. "Adaptive deep learning for head and neck cancer detection using hyperspectral imaging." Vis. Comput. Ind. Biomed. Art **2** (18), (2019)

[5] H. Liang, "Advances in Multispectral and Hyperspectral Imaging for Archaeology and Art Conservation", Appl. Phys. A, **106** (2) (2011).

[6] J. R. J. van Asperen de Boer, "Infrared Reflectography: a Method for the examination of paintings", Appl. Opt., **7**(9), (1968).

[7]   J. Sandak, A. Sandak, L. Legan, K. Retko, M. KavÄiÄ, J. Kosel, F. Poohphajai, R. H. Diaz, V. Ponnuchamy, N. SajinÄiÄ, O. Gordobil, Ärtomir Tavzes, and P. Ropret, " Nondestructive Evaluation of Heritage Object Coatings with Four Hyperspectral Imaging Systems", Coatings, **11** (1), (2021).

[8]   L. de Viguerie, N. Oriols Pladevall, H. Lotz, V. Freni, N. Fauquet, M. Mestre, P. Walter and M. Verdaguer, "Mapping pigments and binders in 15th century Gothic Works of art using a combination on visible and near infrared hyperspectral imaging", Microchem J, **155,** (2020).

[9]   V. Bayarri, M. A. Sebastián and S. Ripoll, "Hyperspectral imaging techniques for the study, conservation and management of rock art", Appl. Sci., **9** (23)**,** (2019).

[10] A. Polak, T. Kelman, P. Murray, S. Marshall, D. J.M. Stothard, N. Eastaugh, F. Eastaugh, "Hyperspectral imaging combined with data classification techniques as an aid for artwork authentication", J. Cult. Herit., **26 ,** (2017).

[11]   B. J. Lindbloom, "Rgb/xyz matrices"
http://www.brucelindbloom.com/index.html?Eqn_RGB_XYZ_Matrix.html

[12]   B. J. Lindbloom, "Chromatic adaptation"
http://www.brucelindbloom.com/index.html?Eqn_ChromAdapt.html
[13]   Mbearnstein37, "Adobe RGB color space: Comparison to sRGB"
https://en.wikipedia.org/wiki/File:CIExy1931_AdobeRGB_vs_sRGB.png
[14]   B. J. Lindbloom, "Gamma correction"
http://www.brucelindbloom.com/index.html?Eqn_XYZ_to_RGB.html
[15]   Thorlabs, "Hyperspectral Imaging System"
https://www.thorlabs.com/newgrouppage9.cfm?objectgroup_id=11095

1. Introduction

As it is widely known, conventional color cameras work by capturing light in three wide bands, later codified as RGB to display the photograph. This allows us to recognize the shape and color of the object in the conditions in which the image was taken, but it does not provide any additional information. However, by measuring the reflectance spectrum of opaque materials we can get more information about said object, such as its chemical composition. This is used in spectroscopy, but it can be invasive. There are non-invasive spectroscopy techniques, but commercial instruments usually present a limitation regarding the size of the sample that can be measured. To solve this, hyperspectral imaging has been developed. This technique consists of photographing the target using a narrow band-pass filter in a wide range of the light spectrum, which allows us to reconstruct the reflectance curve.

Hyperspectral imaging was developed by NASA [1,2] to map mineral or plant distributions on Earth from space, but it has been used in a lot of different fields since then, such as agriculture [3] or biomedicine [4]. We have focused on its use for the analysis of artwork [5].

This technique has been used to observe sketches under the paint and damage in paintings that have been repaired, and to improve the legibility of old documents, in which the ink has deteriorated. To do this, the wavelength range needs to cover the infrared, up to 2 μm, as pigments are transparent in the range from 1 μm to 2 μm [6].

Another application that has been found useful is the renderization of a picture in different illumination conditions, which cannot be done with a conventional camera unless the illumination is changed manually to retake the photograph. Hyperspectral cameras obtain the reflectance spectrum of each pixel, which allows us to choose the illumination with which to render the color image.

This technique could also replace spectroscopy in the analysis of materials, as every element has a different response to electromagnetic radiation, known as spectral signature. Hyperspectral imaging would be a non-invasive identification method [7], as it does not need a sample to be taken. This identification becomes more complicated when there is a mixture of pigments in the artwork analyzed, but there are some methods that have been developed to do it [8]. An advantage of hyperspectral imaging over spectroscopy is that it allows a study of the spatial distribution of the pigments to be made.

Other uses could be the monitoring of artwork [9] or helping with artwork authentication [10]. For this last use, it would be necessary the creation of an extensive database of different pigments used in different periods of history.

The purpose of our work is to build a hyperspectral camera and to develop any necessary software for image processing, and to see if we can obtain a correct color representation with a small number of wavelength bands in the visible range.

This work shows that it is possible to build a hyperspectral camera using affordable discreet components, and we have achieved a system more than 40,000€ cheaper than commercial setups. This camera can be used to simulate artwork in different conditions of illumination and in the future it will be studied its use to identify and classify different pigments and varnishes used in art.

2. Theoretical background

Hyperspectral imaging operates by measuring the light that reaches the camera in numerous narrow wavelength bands that cover a specific range of the light spectrum. By comparing this intensity to the intensity measured when using a white reference target, we can obtain the reflectance spectrum of the target, considering said target opaque. One of the biggest advantages of hyperspectral imaging is that the reflectance spectrum is calculated for each pixel. This gives us more information than other techniques such as spectroscopy, as we can obtain the spatial distribution of the materials from the sample.

In case of not having an ideal white target, the reflectance of the reference white must be taken into consideration when calculating the reflectance spectrum of our target. Said reflectance can be calculated with Equation (1), where I_t is the intensity measured with the target, I_W is the intensity measured with the reference white, I_{BG} is the intensity measured in a black capture and $R_W(\lambda)$ is the reflectance of the reference white for a specific λ. In this work, we have considered the dark noise correction, I_{BG}, as zero.

$$R(\lambda) = \frac{I_t(\lambda) - I_{BG}(\lambda)}{(I_W(\lambda) - I_{BG}(\lambda))/R_W(\lambda)} \tag{1}$$

The reflectance spectrum provides us a lot of information concerning the material under study, but we can also be interested in rendering the image in different illumination conditions, or just in displaying it on the screen. To do that, we need to calculate the color coordinates, starting with the XYZ coordinates that are calculated using Equations (2), (3) and (4). In these equations, $R(\lambda)$ is the reflectance spectrum that we have calculated using Equation (1), $S(\lambda)$ is the illuminant that describes the illumination conditions we want to simulate and $\overline{x}(\lambda)$, $\overline{y}(\lambda)$ and $\overline{z}(\lambda)$ are the tristimulus for a standard observer defined by the International Commission on Illumination (Comission Internationale de l'Eclairage, CIE). We have used the D65 illuminant and the tristimulus for the 10º observer.

$$X = 100 \frac{\int_{380}^{780} R(\lambda)S(\lambda)\overline{x}(\lambda)d\lambda}{\int_{380}^{780} S(\lambda)\overline{y}(\lambda)d\lambda} \tag{2}$$

$$Y = 100 \frac{\int_{380}^{780} R(\lambda)S(\lambda)\overline{y}(\lambda)d\lambda}{\int_{380}^{780} S(\lambda)\overline{y}(\lambda)d\lambda} \tag{3}$$

$$Z = 100 \frac{\int_{380}^{780} R(\lambda)S(\lambda)\overline{z}(\lambda)d\lambda}{\int_{380}^{780} S(\lambda)\overline{y}(\lambda)d\lambda} \tag{4}$$

Once the XYZ coordinates are obtained, they can be transformed into different color coordinates, such as CIELAB or RGB coordinates. CIELAB coordinates can be used to quantify the color difference between two samples, due to their higher uniformity. The transformation between XYZ and CIELAB coordinates is given by Equation (5), where X_n, Y_n and Z_n are the XYZ coordinates of the white point used as reference.

$$\begin{aligned} L^* &= 116 \cdot f(Y/Y_n) - 16 \\ a^* &= 500[f(X/X_n) - f(Y/Y_n)] \\ b^* &= 200[f(Y/Y_n) - f(Z/Z_n)] \end{aligned} \tag{5}$$

$$\text{Where} \quad f(t) = \begin{cases} t^{1/3} & \text{if } t > (6/29)^2 \\ \frac{1}{3}\left(\frac{29}{6}\right)^2 t + \frac{4}{29} & \text{if } t \leq (6/29)^2 \end{cases}$$

Given two different colors with coordinates (L_1^*, a_1^*, b_1^*) and (L_2^*, a_2^*, b_2^*), the color difference ΔE can be calculated as:

$$\Delta E = \sqrt{(L_1^* - L_2^*)^2 + (a_1^* - a_2^*)^2 + (b_1^* - b_2^*)^2} \tag{6}$$

RGB coordinates allow for the image display on a screen. The transformation from XYZ to RGB coordinates consists of a linear transformation, done via a conversion matrix (that we found in [11]), followed by a non-linear transformation, called gamma correction. Conversion matrices are defined for specific illuminants, so if a non-standard illuminant has been used, it is necessary to apply a chromatic adaptation. In our case, we have used the Bradford method [12]. This method uses a predefined transformation matrix, $[M_A]$, which is used to recalculate the color coordinates, XYZ, referred to the white color coordinates of a standard illuminant. The subscript "S" refers to the coordinates calculated with Equations (2), (3) and (4), and the subscript "D" refers to the coordinates referred to the standard illuminant, in Equations (7) and (8).

$$\begin{bmatrix} X_D \\ Y_D \\ Z_D \end{bmatrix} = [M] \begin{bmatrix} X_S \\ Y_S \\ Z_S \end{bmatrix} \tag{7}$$

$$[M] = [M_A]^{-1} \begin{bmatrix} \rho_D/\rho_S & 0 & 0 \\ 0 & \gamma_D/\gamma_S & 0 \\ 0 & 0 & \beta_D/\beta_S \end{bmatrix} [M_A] \tag{8}$$

$(\rho_i, \gamma_i, \beta_i)$ are the coordinates in the conic response domain, and they are calculated using Equation (9), where i = D, S. In this equation, X_W, Y_W and Z_W are the white coordinates, which can be calculated with Equations (2), (3) and (4) using $R(\lambda) = 1 \; \forall \lambda$.

$$\begin{bmatrix} \rho_i \\ \gamma_i \\ \beta_i \end{bmatrix} = [M_A] \begin{bmatrix} X_{Wi} \\ Y_{Wi} \\ Z_{Wi} \end{bmatrix} \tag{9}$$

Once the coordinates are expressed in relation to a standard illuminant, the RGB conversion matrix can be applied. These matrices are defined for a specific color space, too. The most common spaces are the sRGB and Adobe. Fig. 1 shows the different ranges that these spaces include.
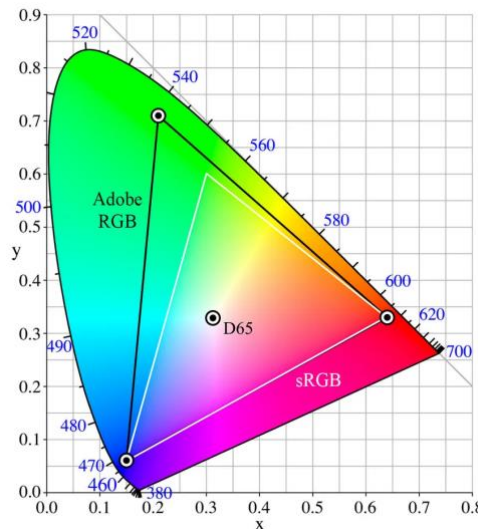

Fig. 1: Comparison of the ranges of the sRGB and Adobe color spaces [13].

The XYZ-RGB conversion is given by Equation (10), where $[M_{RGB}]$ is the matrix defined for a standard white and a specific color space.

$$\begin{bmatrix} r \\ g \\ b \end{bmatrix} = [M_{RGB}] \begin{bmatrix} X \\ Y \\ Z \end{bmatrix} \tag{10}$$

These RGB coordinates are linear, but screens use a non-linear codification. Therefore, it is necessary to implement a gamma correction [14] as defined by Equation (11), wherein the linear coordinates (r, g, b) are denoted as 'v' and the non-linear coordinates (R, G, B) are represented as 'V'. The specific value of the gamma coefficient may differ across screens; for this particular scenario a value of 2.4 has been employed.

$$V = \begin{cases} 12.92v, & if \; v \leq 0.0031308 \\ 1.055v^{1/\gamma} - 0.55, & otherwise \end{cases} \quad \textbf{(11)}$$

With this equation, the values obtained for the RGB coordinates are in the range (0, 1), but they could be rescaled if required.

3. Methodology

The lab setup is composed by a monochrome CMOS USB3.0 MIGHTEX camera, Ocean Insight's LVF-HL linear variable filter, a 60 mm linear stage with a piezoelectric motor from Thorlabs, two white Cree LEDs, two short-focal lenses and a narrow 2 mm aperture to better select the wavelength band that gets to the camera. This setup is shown in Fig. 2, and the prices of the different components are shown in Table 2.
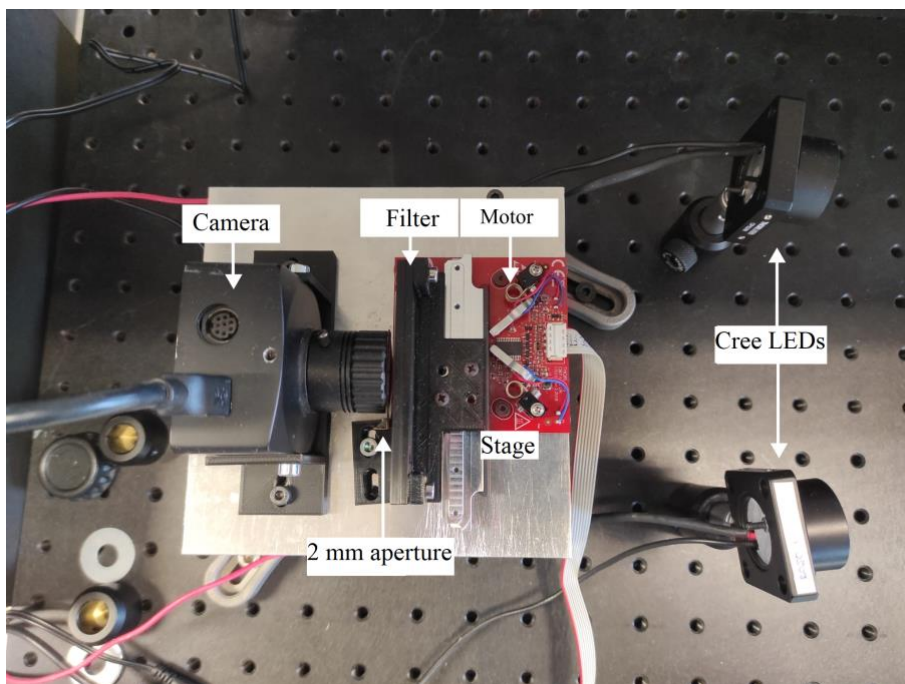

Fig. 2: Lab setup of the hyperspectral camera.

	Units	Price/unit (€)	Price (€)
Camera	1	889.00	889.00
Filter	1	693.00	693.00
Linear stage	1	380.89	380.89
Cree LED	2	2.88	5.76
Lens	2	23.00	46.00
Aperture	1	10.00	10.00
Total			2,024.65

Table 1: Components used for the lab setup of the hyperspectral camera.

Comparing the total price of our system with commercial systems, such as the hyperspectral imaging system sold by Thorlabs [15] for around 47,000€, our setup is more affordable with a similar wavelength range.

The choice of light source was made considering the intensity obtained as well as the spectral range of the light. Cree LEDs cover the range from 410 nm to 790 nm approximately, as it can be seen in Fig. 3. This range is enough for our camera, as the values of the tristimulus are very low in the range from 380 nm to 410 nm and from 700 nm to 780 nm. Therefore, the peaks of the bands measured go from 410 nm to 700 nm. In Fig. 3, the names in the legend refer to the position of the linear stage that moves the filter to select the wavelength band that is transmitted. The first position corresponds to the stage being displaced 18 mm from its home position, and the stage moves in 1 mm steps. The spectra were measured using a spectroradiometer positioned in the camera's location. To ensure that only the band measured with this instrument reaches the camera when photographing an object, the 2 mm aperture was introduced. The measurements obtained with the spectroradiometer were also made using this aperture.
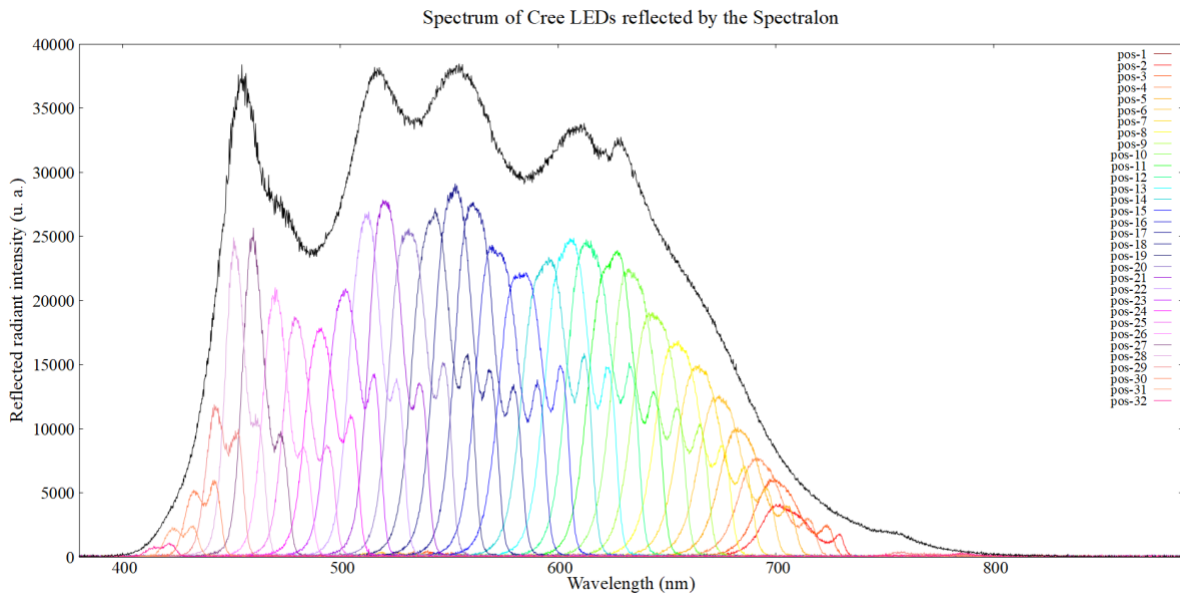

Fig. 3: Cree LEDs spectrum, alongside the bands that the filter lets pass in each position of the stage.

Intensity in the limits of the spectrum decreases very fast, so there is barely any intensity around 400 nm, but the contribution of IR light that the filter lets pass is less prominent than the one obtained with other light sources, such as a halogen lamp.

The characterization of the filter consisted of finding the relation between the position of the stage and the peak wavelength that the filter transmits, and measuring the bands that are transmitted in each position of the stage. The relation among wavelength and position has been obtained by calculating a linear fit of the peak wavelengths measured for each position, which can be seen in Equation (12).The transmittance of the filter can be seen in Fig. 4, where the noise in the limits of the figure is due to the low intensity of light on both the intensity measured with the filter and without it. The wavelength range of the filter is from 300 nm to 750 nm, but the available illumination only allowed for reasonable measurements in the range from 410 to 700 nm, due to the elevated signal-to-noise ratio (SNR). If a UV lamp were to be incorporated, wavelengths between 300 to 410 nm could be measured. However the presented setup does not include it. Fig. 4 also shows how the filter transmits wavelength bands over 750 nm at positions where it should only transmit short wavelengths, between 410 and 450 nm, for example at position 29. These wavelength bands pose a source of error, as their magnitudes are comparable to the bands that we intend to measure.

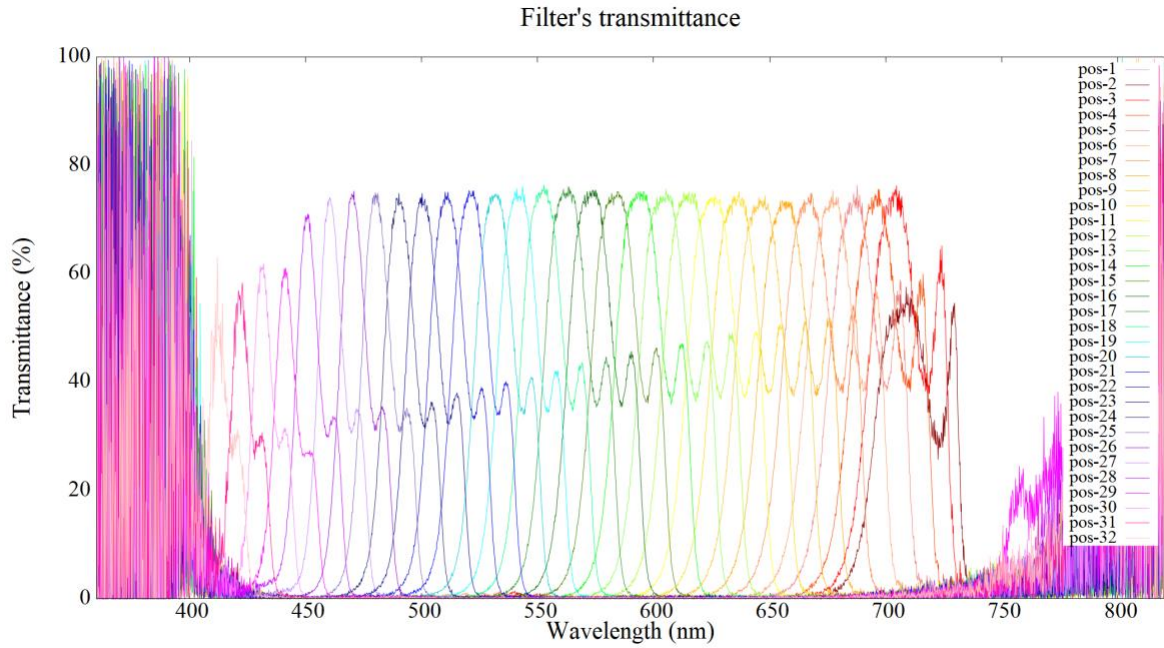$$\lambda(nm) = (-9.50 \pm 0.10) \cdot Pos(mm) + (886 \pm 5) \qquad \textbf{(12)}$$

Filter's transmittance

Fig. 4: Transmittance of the filter in each position of the linear stage.
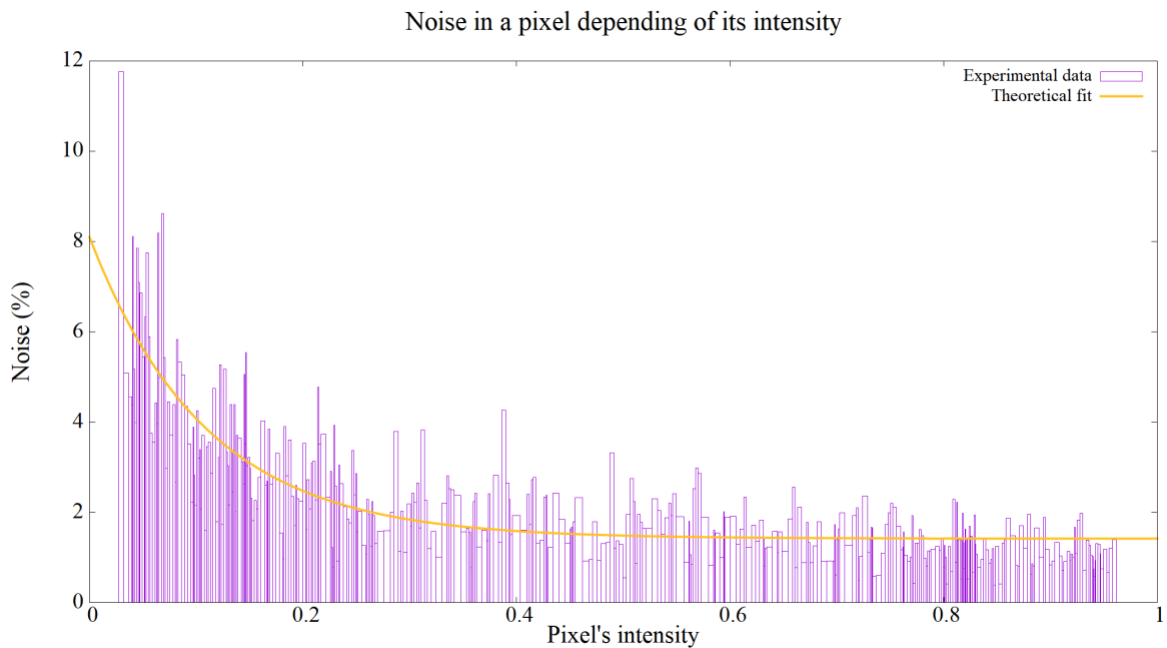
Noise in a pixel depending of its intensity

Fig 5: Noise in a pixel for each possible value of normalized intensity.

The next step involved characterizing the noise as a function of the radiant intensity reaching the camera. In this modelling we have considered that every pixel has the same behavior. To characterize the noise, 20 images were taken with the same exposure time and in the same position. The standard deviation of the values in a determined pixel represents the noise. Comparing this noise for different values of intensity in the pixel, it can be seen that there is a relation between the normalized intensity and the noise presented, as it is shown in Fig. 5. The noise has been modelled as an exponential function, and a fit has been calculated to obtain the parameters of the function, as shown in Equation (13).

$$\text{Noise}(I) = a \cdot e^{-bI} + c \rightarrow \begin{cases} a = 6.7 \pm 0.4 \\ b = 9.2 \pm 0.7 \\ c = 1.41 \pm 0.06 \end{cases} \qquad \textbf{(13)}$$

The final task entailed verifying the linearity between the measured intensity and the exposure time. To accomplish that, the intensity was measured for different exposure times, and the result was that it was linear until the intensity reached 255, which is the maximum value of pixels in the 8-bit images employed.

Once the characterization of the setup was done, six color samples were photographed to test and calibrate the camera. These images were taken with different exposure times, so that the highest non-saturated value could be taken for each pixel. This was done to reduce the noise in the image as much as possible. Various images were taken with the same parameters, so that they could be averaged with the same purpose. The image-processing software performs these steps for each pixel and each position, so that in the end there is only a matrix per position with the maximum value of each pixel, which is normalized by dividing by the corresponding exposure time in each pixel. Doing this for all the positions of the linear stage, the cubic image is constructed and saved in a hypermatrix, or a 3D matrix. This process is performed for each color sample and for a white sample used as reference.

After both hypermatrices are constructed, the software implements the steps and equations explained in **section 2** in each pixel. This software was developed in Matlab, as it allows us to work with big hypermatrices without slowing down the process and it has an extensive library to work with image files.

4. Results

One of the most important things was to make sure that the camera could reconstruct the reflectance spectrum. To evaluate this, this curve was measured for the six color samples using first a colorimeter and then our camera. The comparison between the results obtained with these two methods can be seen in Fig. 6. The spectrum calculated with the camera differs a lot from the one measured with the colorimeter in the range around 400 to 450 nm. This is due to the IR transmitted band that appears in this range. Its intensity is small, but the intensity of the LEDs is also low for wavelengths below 440 nm, so they are comparable.
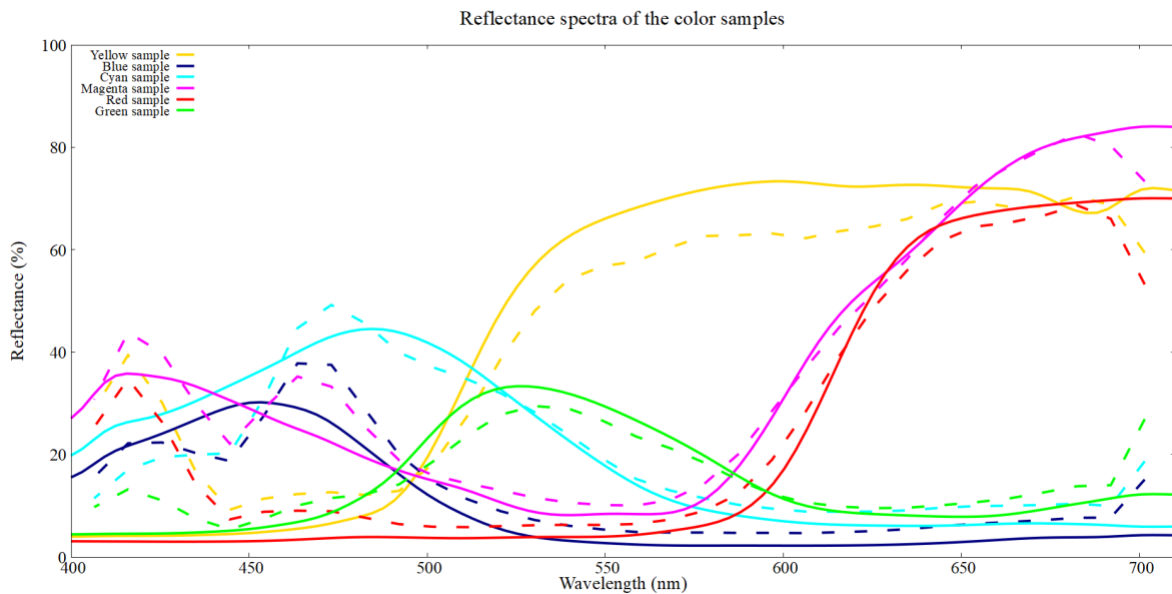

Fig. 6: Reflectance spectra of the color samples, obtained with the hyperspectral camera (dashed lines) and a commercial colorimeter (solid lines).

As the tristimulus have a very low value in the range 400-450, the inaccuracy in the reflectance spectrum barely affects the color rendered, as it can be seen in Fig. 7. The images acquired through the colorimeter correspond to a single reflectance spectrum, and therefore the results obtained with the camera have been averaged for an area comparable to the one measured with the colorimeter. However, each pixel of the images obtained corresponds to a different reflectance spectrum, which explains why the colors in the camera images are not uniform, as the illumination was not homogeneous in the plane of the target, due to the emissivity distribution of the LEDs used to illuminate the setup. To render the colors, the illuminant D65 and the 10º observer tristimulus have been used.

a) Yellow sample   b) Blue sample   c) Cyan sample

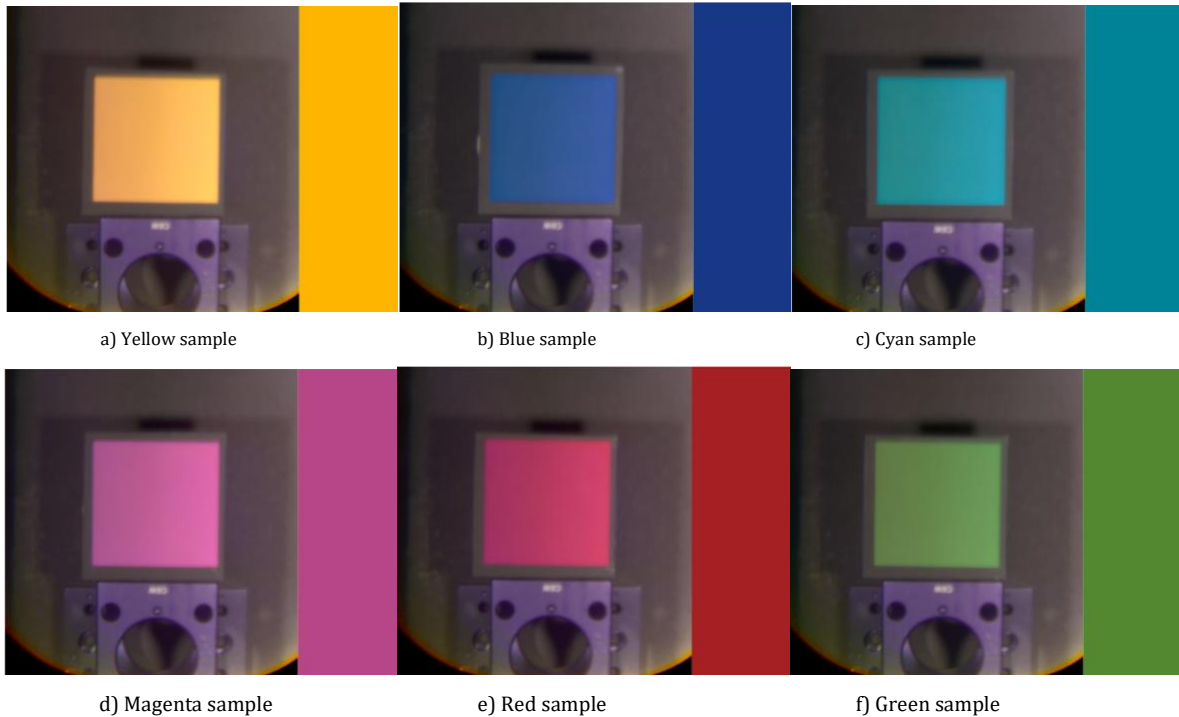d) Magenta sample   e) Red sample   f) Green sample

Fig. 7: Comparison of the colors rendered from the reflectance spectrum obtained with the camera (on the left) and with the colorimeter (on the right).

	L*	a*	b*	ΔE	ΔR$_{vis}$ (%)
Yellow (camera)	75.3 ± 1.1	9.8 ± 0.6	50.0 ± 1.3	31.7 ± 1.3	7.1 ± 0.5
Yellow (colorimeter)	78.4	14.7	81.2		
Blue (camera)	35.8 ± 0.5	0.9 ± 0.6	-37.2 ± 0.8	22.8 ± 0.6	3.0 ± 0.1
Blue (colorimeter)	25.9	18.9	-47.1		
Cyan (camera)	53.4 ± 0.6	-30.9 ± 0.3	-14.2 ± 0.9	10.2 ± 0.5	0.7 ± 0.2
Cyan (colorimeter)	50.1	-22.6	-19.2		
Magenta (camera)	52.0 ± 0.8	38.9 ± 0.7	-15.4 ± 0.5	14.5 ± 0.7	2.0 ± 0.2
Magenta (colorimeter)	47.2	52.4	-12.9		
Red (camera)	42.6 ± 0.8	45.9 ± 0.6	2.7 ± 1.2	32.0 ± 1.2	2.6 ± 0.1
Red (colorimeter)	36.3	52.7	33.3		
Green (camera)	51.7 ± 0.8	-27.5 ± 0.9	26.1 ± 0.5	15.3 ± 0.6	2.0 ± 0.2
Green (colorimeter)	51.1	-33.3	40.2		

Table 2: Comparison of the results obtained with the colorimeter and the camera, where ΔR$_{vis}$ is calculated as the difference between the visible reflectance obtained from the colorimeter's spectrum and the visible reflectance from the camera's spectrum.

As it can be seen in Fig. 7, the colors are not the same, due to the differences in the reflectance spectra. This is shown in Table 2, which presents the L*a*b* coordinates of the colors obtained with the colorimeter and the ones obtained for an average of the pixels in an area similar to the area measured by the colorimeter. This table also shows the color difference ΔE calculated using Equation (6) and the difference of global visible reflectance obtained with the reflectance spectra of the colorimeter and the camera. The difference in the coordinates is significant in most cases, being the biggest source of error the coordinate corresponding to the color range in which we can see the most discrepancy in Fig. 6. For example, in the yellow sample the biggest difference between the coordinates for the camera and the colorimeter is in the coordinate b*, which represents the position between blue and yellow. The discrepancy in this coordinates is due to the increase in the spectrum of the yellow sample in the range of 400 to 450 nm. This rise is probably caused by the IR light that the filter transmits in this range. However, despite the discrepancies, the colors obtained are very similar and recognizable. Regarding the disparity

in visible global reflectance, it is noticeable that it never exceeds 10%. However, in some cases, it closely approximates said value.
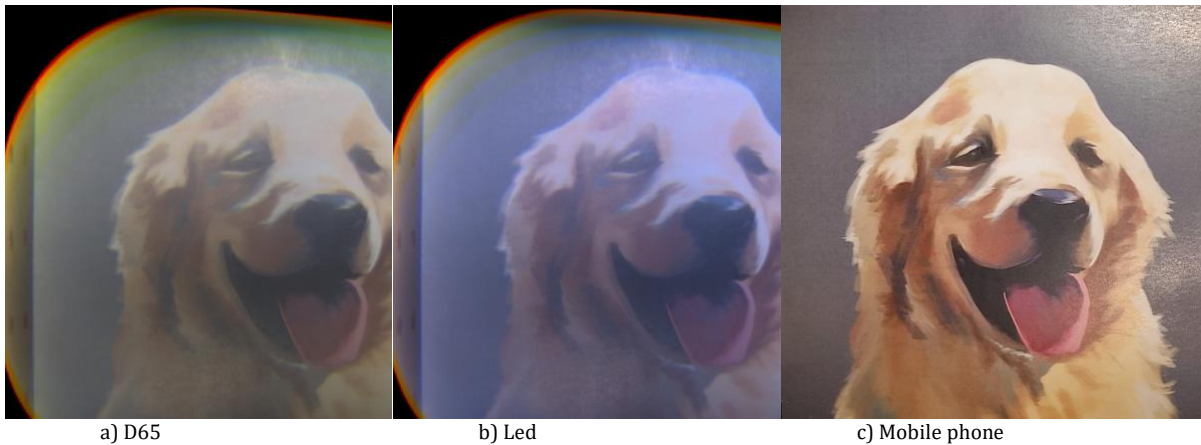

| a) D65 | b) Led | c) Mobile phone |

Fig. 8: Comparison of the results obtained with the hyperspectral camera with two different illuminants (a and b) and with a mobile phone (c). Illustration made by the artist Eva Gutiérrez (newev).

To conclude, we measured an illustration to determine whether similar colors are rendered differently. Fig. 8 shows the image obtained with our camera using two different illuminants and with a mobile phone. The image obtained with the phone shows higher contrast and brightness, but these are due to the automatic corrections implemented by the phone. These corrections could be implemented in our system, but it is left as a future improvement. We can see that the hyperspectral camera allows us to discern between similar colors and we have been able to render the image under two different conditions of illumination. The resulting images present some of the aberrations of low-cost optics, such as vignetting, chromatic aberration and reduced image acuity. The vignetting is probably due to the presence of the 2 mm aperture, which reduces the camera's field of view. However, as the aperture ensures selected transmission of the desired wavelength band to the camera, rectifying this defect has not been possible. Regarding both the chromatic aberration and the lack of sharpness, it is attributable to the simplicity of the optical system, and correcting it would involve significantly complicating the laboratory setup.

5. Conclusions

We have proven that it is possible to build a system capable of reconstructing the reflectance spectrum using a small number of bands even in images with a high contrast in reflectance. We have also shown that the difference in the global visible reflectance between the reconstructed reflectance spectra and the reflectance spectra measured with the colorimeter is lower than it could be expected, given the aberrations introduced by the simple system of low-cost optics implemented. Lastly, we have managed to successfully simulate images in different conditions of illumination.

This setup could be improved by adding an infrared filter that eliminates the contribution of the IR bands that appear when the filter lets pass bands below 450 nm (for example, the band at 750 nm shown in Fig. 4, that corresponds to position 29 of the filter). It could also be beneficial to find a light source that reaches wavelengths a bit below 400 nm, or that at least has a higher intensity around 400 nm. This would reduce the error in the spectrum in the range of 400 to 450 nm, allowing for a better renderization of blue colors. It could also be beneficial to introduce digital corrections to the images obtained, in order to counteract some of the aberrations present in our imaging system.